Electronic Supplementary Material (ESI) for Environmental Science: Nano.

A New Compound $Mn_5P_4O_{20}H_8$ Achieving Efficient Heavy Metals Removal to ppb Level through A Dual Chemisorption-ion exchange Pathway

Mingxia Deng, [a,b] *Weijing Liu,*[c] *Qian Liu,* [*a] *Du Sun,* [*a] *and Fuqiang Huang*[*a,b,d]

[a] *State Key Laboratory of High Performance Ceramics and Superfine Microstructure, Shanghai Institute of Ceramics, Chinese Academy of Sciences, Shanghai 200050, P. R. China;*

[b] *Center of Materials Science and Optoelectronics Engineering, University of Chinese Academy of Sciences, Beijing 100049, China;*

[c] *Jiangsu Provincial Key Laboratory of Environmental Engineering, Jiangsu, China*

[d] *Beijing National Laboratory for Molecular Sciences and State Key Laboratory of Rare Earth Materials Chemistry and Applications, College of Chemistry and Molecular Engineering, Peking University, Beijing 100871, P. R. China.*

E-mail Address: mailto:huangfq@mail.sic.ac.cn(Fuqiang Huang)

mailto:sundu@mail.sic.ac.cn (Du Sun)

mailto:qianliu@mail.sic.ac.cn(Qian Liu)

mailto:liuwj@jshb.gov.cn(Weijing Liu)

mailto:mingxiadeng@student.sic.ac.cn(Mingxia Deng)

Table S1. Adsorption equilibrium concentration of different adsorption materials

Sample		Metal ions	C_0	C_e	References
Metal oxides	MoS_4-LDH	As(V)	16.84 ppm	0.31 ppm	***A***
	MoS_4-LDH	Cr(VI)	19.4 ppm	0.01 ppm	***A***
	CoAl-LDH	Cr(VI)	26.29 ppb	**0.012 ppb**	***B***
	CoAl-LDH	Cr(VI)	12.36 ppm	0.28 ppm	***B***
	$(MgO)_{2.9}MnO_2$	Hg(II)	1500 ppb	**5 ppb**	***C***
	$(MgO)_{2.9}MnO_2$	Pb(II)	500 ppb	**2 ppb**	***C***
	titanate nanotubes (TNTs)	Pb(II)	621 pm (3mol/L)	41 ppm (0.19mol/L)	***D***
	titanate nanotubes (TNTs)	Cr(III)	156ppm (3mol/L)	135 ppm (2.6mol/L)	***D***
Carbon-based materials	HOTT-HATN	Pb(II)	10 ppm	**<0.60 ppm**	***E***
MOF-based materials	ED-MIL-101	Pb(II)	414 ppm (2 mol/L)	384 ppm (1.86mol/L)	***F***
	Zn(hip)(L)·(DMF)(H2O)	Hg(II)	20 ppb	**3.05 ppb**	***G***
Functional polymers	PVBH	Cu(II)	50 ppb	18 ppb	***H***
	PVBH	Cr(III)	50 ppb	**0.05 ppb**	***H***
	CoS_2/GO	Hg(II)	34 ppb	**2 ppb**	***I***

	CoS_2/GO	Hg(II)	102.50 ppm	18.84 ppm	***I***
	NFM	Pb(II)	~100 ppb	**1.41 ppb**	***J***
	NFM	Pb(II)	9.07 ppm	**38 ppb**	***J***
Our work	**$Mn_5P_4O_{20}H_8$**	**Pb(II)**	**2.31 ppm**	**1 ppb**	
	$Mn_5P_4O_{20}H_8$	**Cr(III)**	**4.38 ppm**	**40 ppb**	
	$Mn_5P_4O_{20}H_8$	**Fe(III)**	**2.34 ppm**	**1 ppb**	

Table S2. Crystallographic Data and Details of the Structure Refinements of $Mn_5P_4O_{20}H_8$

Empirical formula	**$Mn_5P_4O_{20}H_8$**
Formula weight (g/mol)	726.64
Space group	*C2/c*
Crystal system	*Monoclinc*
Unit cell	*a* = 17.6182(8) Å
	b = 9.1333(4) Å
	c = 9.4921(4) Å
□	96.532(2)°
Volume (Å^3)	1517.48(12) Å^3
Z	16
F(000)	1412
***θ* range (°)**	2.3-30.6
Reflections collected	2328
Independent reflections	149
Calculated density (g/cm^3)	3.181
μ (mm^{-1})	4.59
crystal color	Light pink
Goodness-of-fit on F^2	1.003
R_{int}	0.049
R_1 for [$I>2\sigma(I)$][a]	0.0214
wR_2 for [$I>2\sigma(I)$][a]	0.0603

a ：R1，wR2 calculation method

[a]$R1 = \Sigma||F_o| - |F_c||/\Sigma|F_o|$, w$R_2 = [\Sigma w(F_o^2 - F_c^2)^2/\Sigma(wF_o^2)^2]^{1/2}$, $w = 1/[\sigma^2(F_o^2) + (aP)^2 + bP]$, where F_o is the observed structure factor, Fc is the calculated structure factor, σ is the standard deviation of F_c^2, and $P = (F_o^2 + 2F_c^2)/3$. $S = [\Sigma w(F_o^2 - F_c^2)^2/(n - p)]^{1/2}$, where n is the number of reflections and p is the total number of parameters refined.

Quartz Crystal Microbalance with Dissipation monitoring (QCM-D):

QCM-D measurements were performed on the commercial Q-Sense Explore

system (Biolin Scientific AB, Sweden). The area of sensor was 0.785 cm^2 (a circle with a diameter of 10 mm). QCM-D can be used to measure the film mass by monitoring changes in frequency and dissipation sensitively of an acoustic resonator. By integrating QCM-D, we can simultaneously measure the real-time mass change of $Mn_5P_4O_{20}H_8$ fil. To this end，a titanium gold-coated AT-cut quartz crystal sensor chips was uniformly coated with an adsorbent slurry, 10 mg $Mn_5P_4O_{20}H_8$ and 200 μL 20 mg/mL PVDF by adding dropwise and then dried at room temperature. The $Mn_5P_4O_{20}H_8$ membrane was first characterized in deionized water at speed of 50 μL/s to establish a baseline for the subsequent mass study. To evaluate the removal process of the new compound for Cr^{3+}, 2 mmol/L Cr^{3+} aqueous solution was used during the Regime 1 and then 1 mol/L HNO_3 was used during the Regime 2, followed by Cr^{3+} aqueous solution for re-adsorption tests.

Experiments of different ratio: A series of phosphorylated manganese oxides were prepared by hydrothermal method. Typically, $Mn(CH_3COO)_2$ was added to 30 mL ethanol in 50 mL beaker, and then slowly stirred at room temperature. After $Mn(CH_3COO)_2$ was dissolved, a certain amount of phosphorus source such as phytic acid and phosphoric acid was added to the above mixture, followed by stirring for 120 min at room temperature. Then the obtained mixture was transferred into a 50 ml Teflon-lined stainless-steel autoclave and subjected to hydrothermal treatment at 150°C for 15h. Finally, the obtained precipitate was centrifuged and then washed with ethanol and deionized water for three times. After the sample was dried under vacuum overnight, A series of phosphorylated manganese oxides was obtained (Figure.S1). The amount of phytic acid were 0.57 mL and 1 mL, and the phosphorus source were phosphoric acid, phytic acid of 50% and 70%. Only 0.57 ml of phytic acid was added, a new compound of $Mn_5P_4O_{20}H_8$ was obtained.

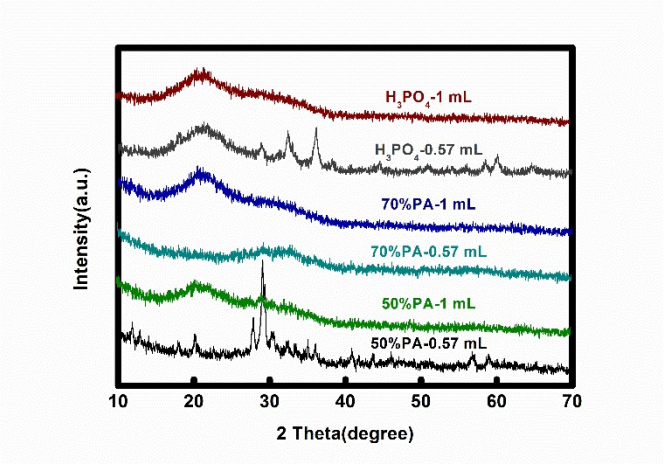

Figure S1. XRD spectrum of different ratio products.

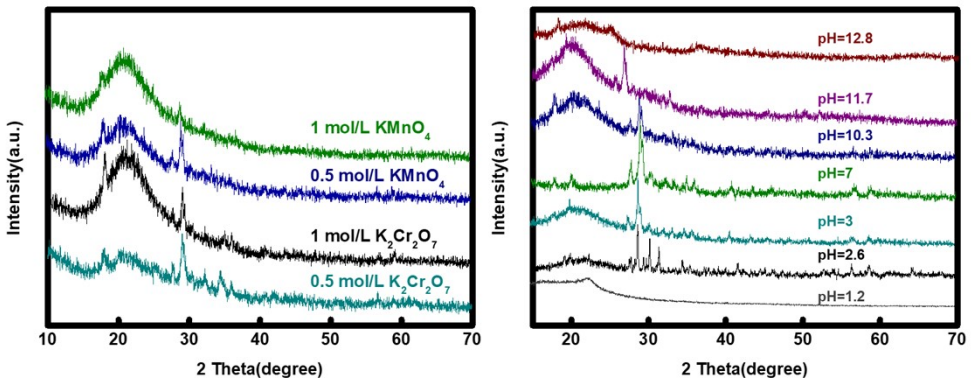

Figure S2. (a) the inoxidizability of $Mn_5P_4O_{20}H_8$; (b)the acid and base stability of $Mn_5P_4O_{20}H_8$ in a wide range of pH values (1.3−12.8)

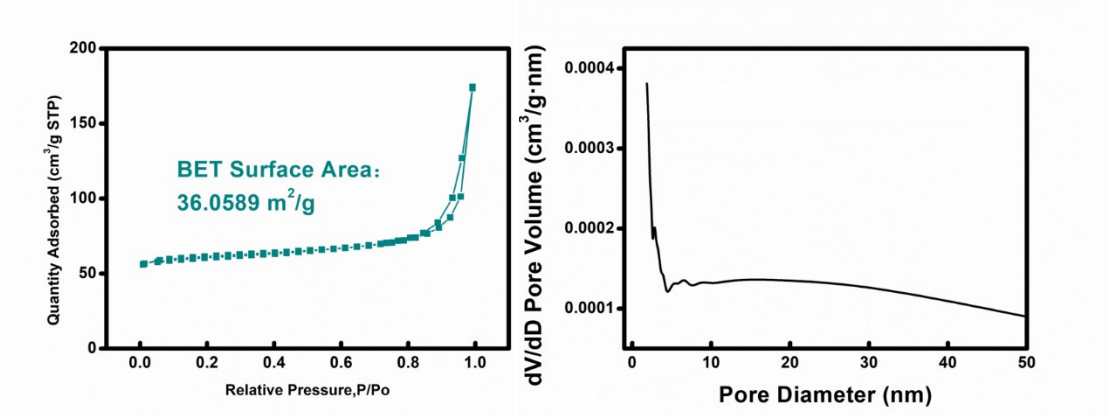

Figure S3. Nitrogen adsorption and desorption curve and pore distribution diagrams of $Mn_5P_4O_{20}H_8$.

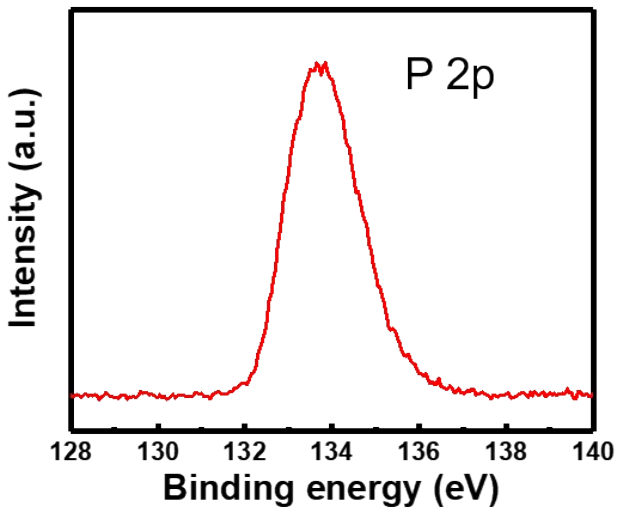

Figure S4. High-resolution XPS spectrum of P 2*p*.

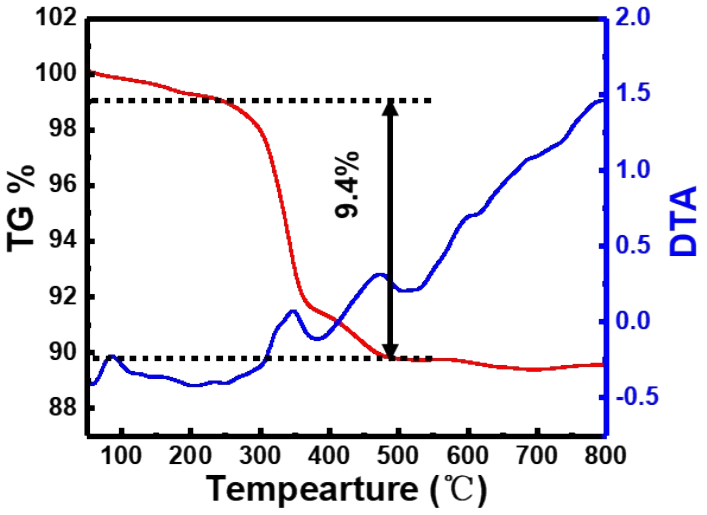

Figure S5. TG curve of $Mn_5P_4O_{20}H_8$.

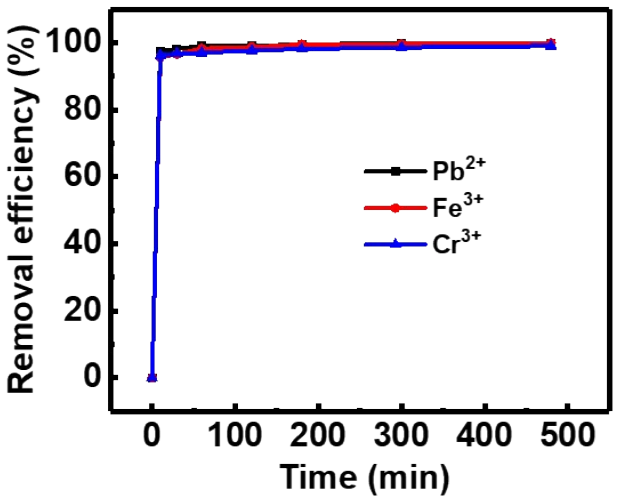

Figure S6. Removal (%) as a function of contact time on $Mn_5P_4O_{20}H_8$.

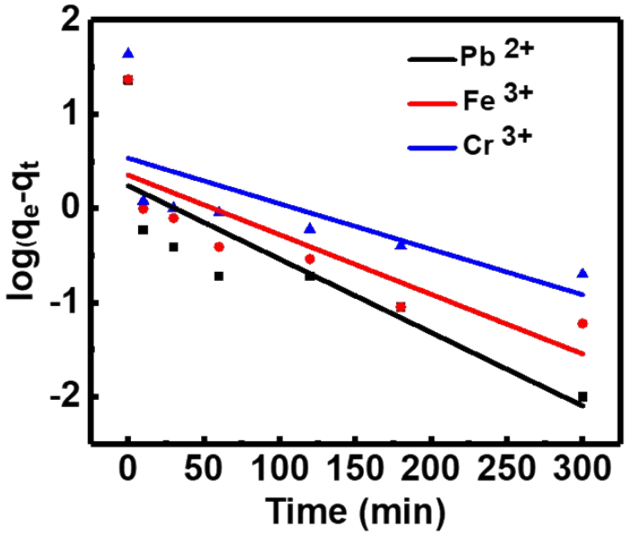

Figure S7. Pseudo- first order kinetics plots of $Mn_5P_4O_{20}H_8$ towards Cr^{3+}, Fe^{3+}, and Pb^{2+}.

Table S3. Kinetic Parameters for the Adsorption of Cr^{3+}, Fe^{3+}, and Pb^{2+} on $Mn_5P_4O_{20}H_8$.

		Pseudo-first order model			Pseudo-second order model		
	$q_{e,exp}$ (mg/g)	k_1 (min^{-1})	$q_{e,cal}$ (mg/g)	R^2	k_2 (min^{-1})	$q_{e,cal}$ (mg/g)	R^2
Cr^{3+}	43	0.0111	3.47	0.4952	0.0199	43.44	0.9998
Fe^{3+}	23	0.1528	2.25	0.6521	0.0399	23.43	0.9999
Pb^{2+}	23	0.1561	1.74	0.7003	0.0687	23.11	0.9999

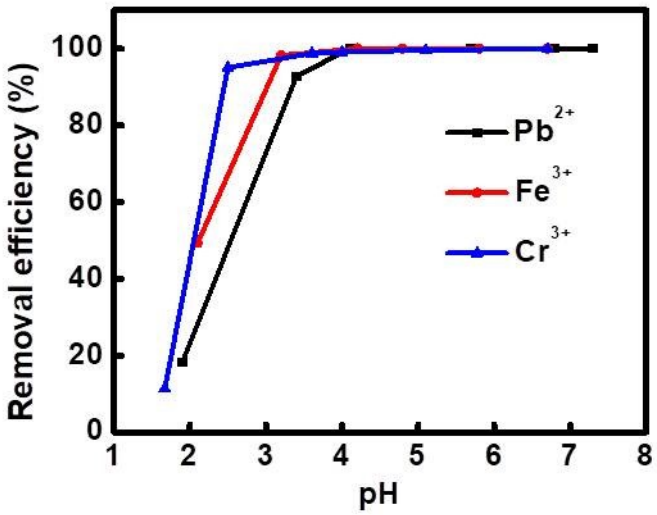

Figure S8. Effect of solution pH on the adsorption on $Mn_5P_4O_{20}H_8$.

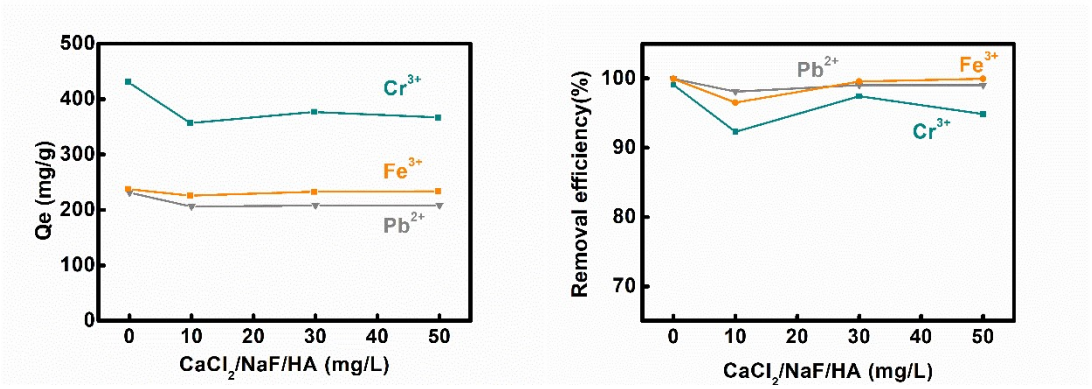

Figure S9. Effect of Effects of coexistence of cation, anion and hyaluronic acid on adsorption of heavy metal ions

Table S4. Parameters of the Langmuir and Freundlich Isotherm for Cr^{3+}, Fe^{3+}, and Pb^{2+} Adsorption on $Mn_5P_4O_{20}H_8$.

	Langmuir model			Freundlich model		
	q_{max} (mg/g)	K_L (L/mg)	R^2	K_F ($mg^{1-n}L^n/g$)	n	R^2
Cr^{3+}	201	2.97	0.9912	162	3	0.7551
Fe^{3+}	300	3.04	0.9882	197	2	0.9599
Pb^{2+}	1510	1.59	0.9969	866	5	0.8991

Table S5. Selectivity results for $Mn_5P_4O_{20}H_8$. in mixed metal solution

	Cr^{3+}	**Fe^{3+}**	**Pb^{2+}**	**Cu^{2+}**	**Ca^{2+}**	**Na^{+}**	**Mg^{2+}**	**Zn^{2+}**
Initial Concentration (ppm)	**5.49**	**5.60**	**6.89**	**5.11**	**5.30**	**5.35**	**5.28**	**5.68**
Equilibrium Concentration (ppm)	**0.72**	**<0.01**	**0.23**	**0.09**	**5.15**	**5.05**	**4.73**	**5.67**
Efficiency (%)	**86.88**	**99.82**	**96.66**	**98.24**	**2.83**	**5.61**	**10.50**	**0.18**

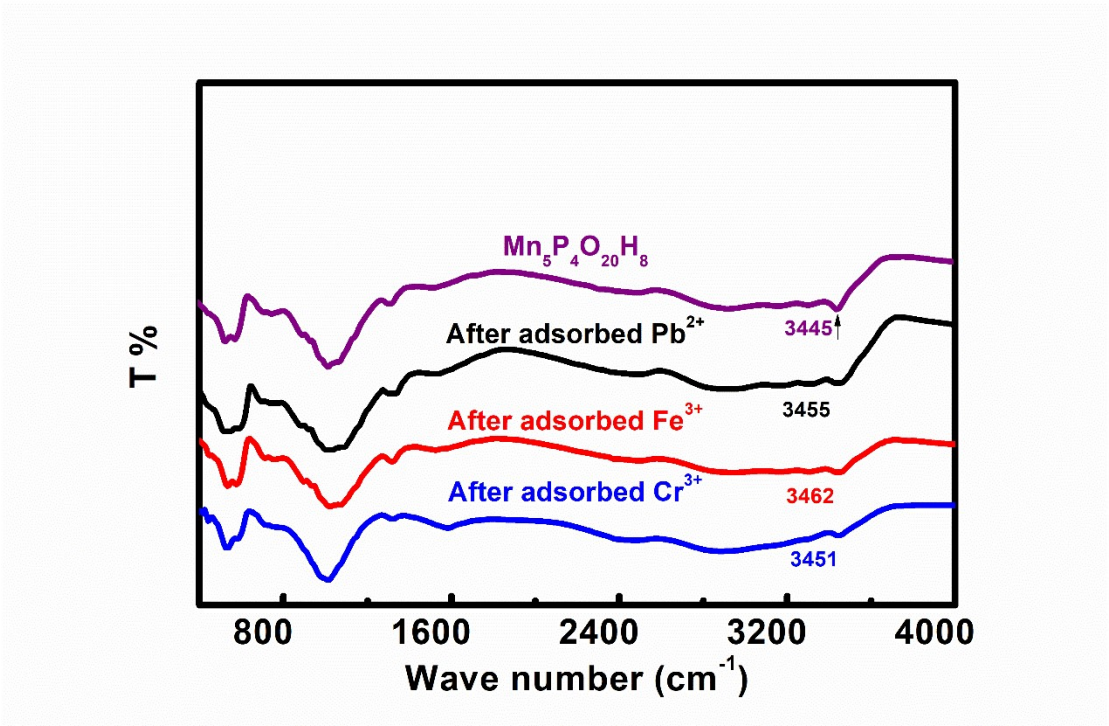

Figure S10. The infrared spectroscopy of $Mn_5P_4O_{20}H_8$ after adsorption

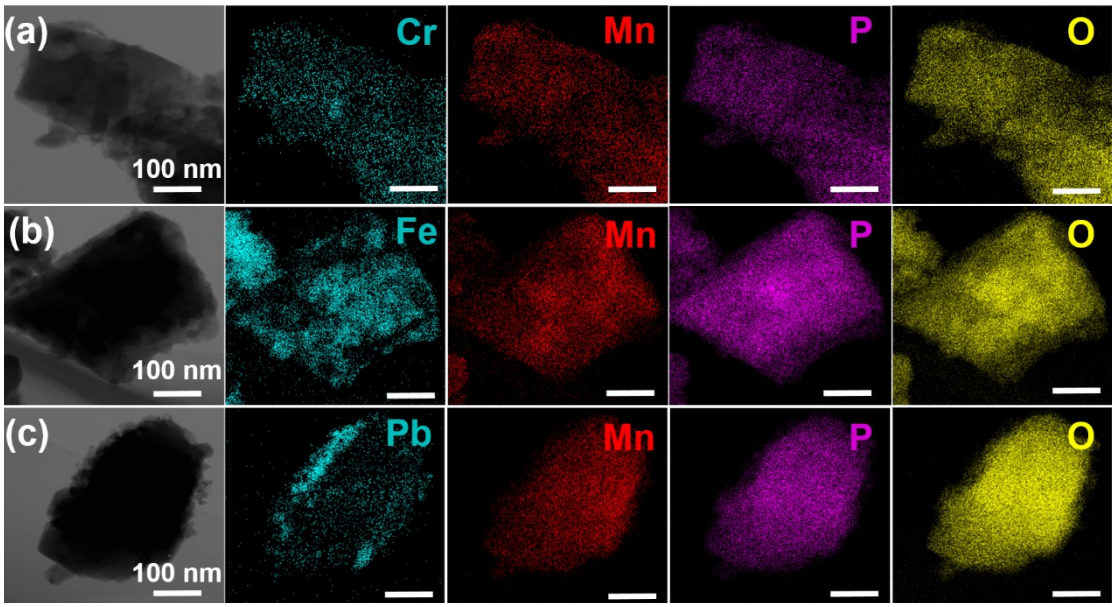

Figure S11. EDX elemental mappings (scale bar, 100 nm) of $Mn_5P_4O_{20}H_{8\ after}$ after adsorption of (a)Cr^{3+}, (b) Fe^{3+}, and (c) Pb^{2+}.

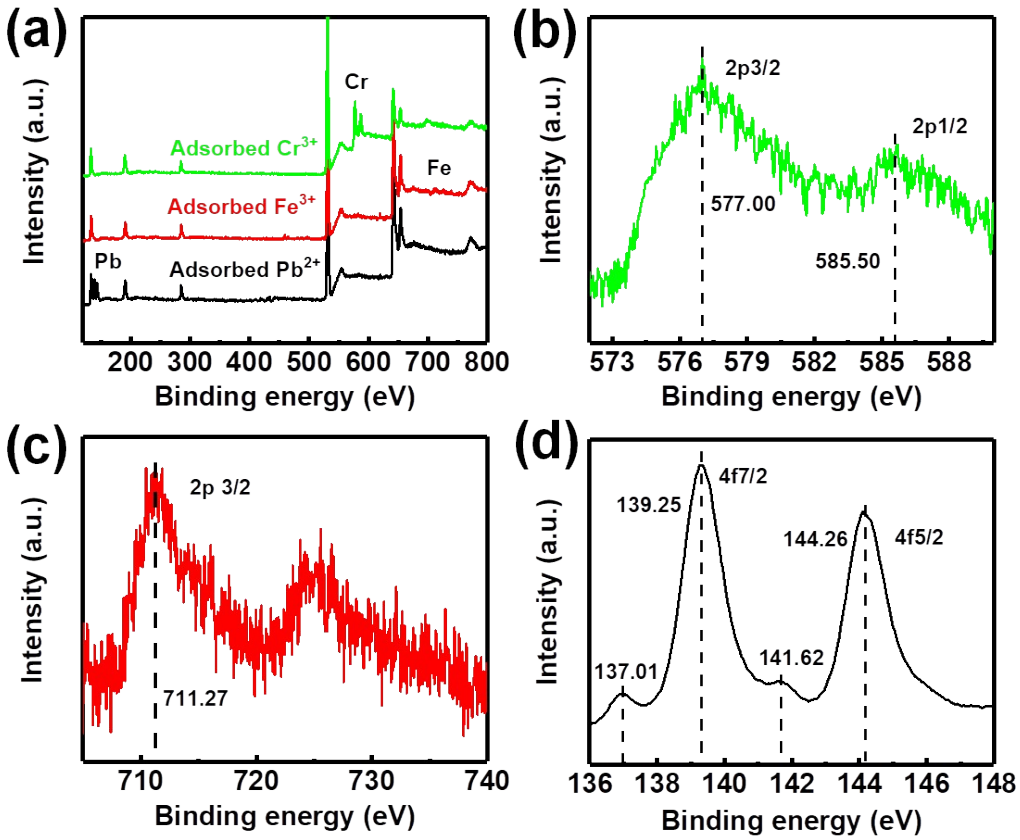

Figure S12. (a) Full XPS spectra of $Mn_5P_4O_{20}H_8$ after adsorbed heavy metal ions; (b), (c) and(d) High-resolution XPS spectra of Cr 2*p*, Fe 2*p*, and Pb 4*f* from $Mn_5P_4O_{20}H_8$ after adsorbed heavy metal ions, respectively

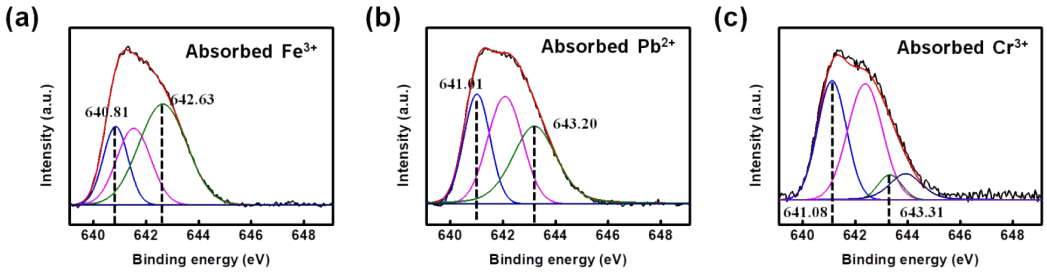

Figure S13. (a), (b) and (c) High-resolution XPS spectra of Mn $2p_{3/2}$ peaks from $Mn_5P_4O_{20}H_8$ after adsorbed Fe^{3+}, Pb^{2+} and Cr^{3+}, respectively

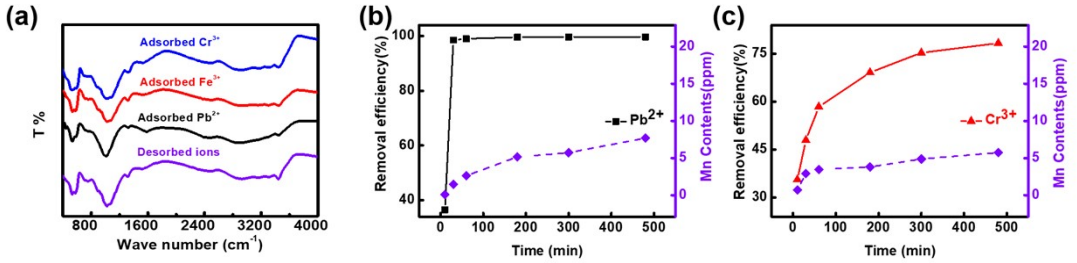

Figure S14. (a) The XRD patterns of $Mn_5P_4O_{20}H_8$ after heavy metal ions adsorption and desorption; (b) and (c) Removal efficiencies of heavy metal ions and Mn ion concentrations in the solution after adsorbed Pb^{2+} and Cr^{3+}, respectively

Table S6. Control experiments of components

	Phytic acid	**Manganese acetate**	**Physical mix of phytic acid and manganese acetate**
Initial Concentration (ppm)	18.1	18.1	23.3
Equilibrium Concentration (ppm)	15.5	17.7	21.7
Efficiency (%)	14.3%	2.2%	6.8%

Table.S7 the relationship between pH of the solution after heavy metal adsorption and the concentration of Mn(II) and Pb(II)

	Pb Concentration (ppm)	**Mn Concentration (ppm)**	**Removal (%)**
pH5.6	**0.2**	**17.1**	
pH6.4	**0.3**	**15.7**	**8.2**

pH7.2	**0.8**	**6.2**	**63.7**
pH8.1(20 min)	**0.4**	**0.9**	**94.7**
pH8.1(2 h)	**0.2**	**0.03**	**99.8**

References

A Ma, L., Islam, S. M., Liu, H., Zhao, J., Sun, G., Li, H., Ma, S., & Kanatzidis, M. G. (2017). Selective and Efficient Removal of Toxic Oxoanions of As(III), As(V), and Cr(VI) by Layered Double Hydroxide Intercalated with MoS42-. Chemistry of Materials, 29(7), 3274–3284.

B Rathore, E., Maji, K., & Biswas, K. (2021). Nature-Inspired Coral-like Layered [Co0.79Al0.21(OH)2(CO3)0.11]· mH2O for Fast Selective ppb Level Capture of Cr(VI) from Contaminated Water. *Inorganic Chemistry*, 2021,*60*(13), 10056–10063.

C P. Askari, A. Faraji, G. Khayatian, S. Mohebbi, Effective ultrasound-assisted removal of heavy metal ions As(III), Hg(II), and Pb(II) from aqueous solution by new MgO/CuO and MgO/MnO_2 nanocomposites, *J. Iran. Chem. Soc*, 2017, 14(3):613-621.

D W. Liu, T. Wang, A.G.L. Borthwick, Y.Q. Wang, X.C. Yin, X.Z. Li, J.R. Ni, Adsorption of Pb2+, Cd2+, Cu2+ and Cr3+ onto titanate nanotubes: Competition and effect of inorganic ions, Science of the Total Environment 456 (2013) 171-180.

E R. Xiao, John M. Tobin, M.Q. Zha, Y.L. Hou, J. He, F. Vilela, Z.T. Xu, A nanoporous graphene analog for superfast heavy metal removal and continuous-flow visible-light photoredox catalysis, J. Mater. Chem. A 5 (2017) 20180- 20187.

F X.B. Luo, L. Ding, J.M. Luo, Adsorptive Removal of Pb(II) Ions from Aqueous Samples with Amino-Functionalization of Metal−Organic Frameworks MIL-101(Cr), J. Chem. Eng. Data 60 (2015) 1732-1743

G Luo, F., Chen, J. L., Dang, L. L., Zhou, W. N., Lin, H. L., Li, J. Q., Liu, S. J., & Luo, M. B. (2015). High-performance Hg2+ removal from ultra-low-concentration aqueous solution using both acylamide- and hydroxyl-functionalized metal–organic framework. Journal of Materials Chemistry A, 3(18), 9616–9620.

H Amoyaw, P. A., Williams, M., & Bu, X. R. (2009). The fast removal of low concentration of cadmium(II) from aqueous media by chelating polymers with salicylaldehyde units. Journal of Hazardous Materials, 170(1), 22–26.

I Wang, Y., Bao, S., Liu, Y., Yu, Y., Yang, W., Xu, S., & Li, H. (2021). CoS2/GO nanocomposites for highly efficient and ppb level adsorption of Hg(II) from wastewater. *Journal of Molecular Liquids*, 2021,*322*, 114899.

J Wei, J., Jiao, X., Wang, T., & Chen, D. (2018). Fast, simultaneous metal reduction/deposition on electrospun a-WO3/PAN nanofiber membranes and their potential applications for water purification and noble metal recovery. Journal of Materials Chemistry A, 6(30), 14577–14586.